



Research Article

Prostaglandin E₂ impacts multiple stages of the natural killer cell antitumor immune response

Chloe Patterson¹, Khodor S. Hazime³ , Santiago Zelenay^{1,2}
and Daniel M. Davis³ 

¹ The Lydia Becker Institute of Immunology and Inflammation, The University of Manchester, Manchester, United Kingdom

² Cancer Inflammation and Immunity Group, Cancer Research UK Manchester Institute, The University of Manchester, Manchester, United Kingdom

³ Department of Life Sciences, Sir Alexander Fleming Building, Imperial College London, South Kensington, London, United Kingdom

Tumor immune escape is a major factor contributing to cancer progression and unresponsiveness to cancer therapies. Tumors can produce prostaglandin E₂ (PGE₂), an inflammatory mediator that directly acts on Natural killer (NK) cells to inhibit antitumor immunity. However, precisely how PGE₂ influences NK cell tumor-restraining functions remains unclear. Here, we report that following PGE₂ treatment, human NK cells exhibited altered expression of specific activating receptors and a reduced ability to degranulate and kill cancer targets. Transcriptional analysis uncovered that PGE₂ also differentially modulated the expression of chemokine receptors by NK cells, inhibiting CXCR3 but increasing CXCR4. Consistent with this, PGE₂-treated NK cells exhibited decreased migration to CXCL10 but increased ability to migrate toward CXCL12. Using live cell imaging, we showed that in the presence of PGE₂, NK cells were slower and less likely to kill cancer target cells following conjugation. Imaging the sequential stages of NK cell killing revealed that PGE₂ impaired NK cell polarization, but not the re-organization of synaptic actin or the release of perforin itself. Together, these findings demonstrate that PGE₂ affects multiple but select NK cell functions. Understanding how cancer cells subvert NK cells is necessary to more effectively harness the cancer-inhibitory function of NK cells in treatments.

Keywords: Cytotoxicity · Cancer · Immune escape · Natural killer cell · Prostaglandin E₂



Additional supporting information may be found online in the Supporting Information section at the end of the article.

Introduction

Natural killer (NK) cells are innate lymphoid cells that have the inherent capacity to recognize and kill foreign, infected, and malignant cells [1]. NK cell effector functions include cellular cytotoxicity and cytokine secretion and thus, they play an important role in early and effective immune responses [2]. Unlike T

lymphocytes, the cytotoxic function of NK cells is regulated by the balance of signals from a diverse repertoire of germline-encoded activating and inhibitory receptors [3]. Upon activation and formation of an immune or immunological synapse, NK cells can directly kill cancer cells by secretion of granules containing perforin and granzyme B [4]. Alternatively, if inhibitory signals dominate, an inhibitory synapse assembles, where the balance of signals cuts short the duration of the contact and prevents NK cell effector functions [5].

Correspondence: Prof. Daniel M. Davis
e-mail: d.davis@imperial.ac.uk

Besides their direct recognition and killing of cancer cells, NK cells are also central orchestrators of T cell immunity and thus, are directly involved in the response to T cell-targeting immune checkpoint inhibition therapies [6]. NK cells can induce a switch in the tumor microenvironment (TME) toward an inflammation which inhibits cancer progression, through the production of mediators including IFN- γ , that stimulate T-cell-mediated immunity [6]. Moreover, NK cells can secrete chemokines that attract myeloid cells to the tumor and promote further T cell recruitment [7].

Intratumoral NK cell frequency correlates with improved prognosis in several different cancers [7–11]. However, some tumors escape immune surveillance and grow despite immune cell infiltration [12]. Tumors can potentiate their own survival and progression through the development of a complex TME [13]. Inflammatory cells and cellular mediators of inflammation are key constituents of the TME and can have many tumor-promoting effects [13]. Accordingly, they constitute adverse prognostic factors and promote therapy resistance [6]. Prominent among tumor-sustaining mediators is prostaglandin E₂ (PGE₂) whose production has been associated with enhancement of cancer cell survival, growth, invasion, angiogenesis, and immunosuppression [14]. Cyclooxygenase (COX)-1 and 2 enzymes are critical for the production of PGE₂ and often overexpressed in colorectal, breast, stomach, lung, and pancreatic cancers [14], where they are associated with decreased survival among cancer patients [6, 15].

The recent success of immunotherapies has reinvigorated the study of tumor immunology and inflammation, and in recent years, NK cells have emerged as a potential target for cancer immunotherapies. They are an attractive alternative to T cell immunotherapies because they preferentially target “altered” cells in the body, without the need for prior sensitization or knowledge of specific cancer cell antigens [9]. However, in order to more successfully harness the cancer inhibitory function of NK cells in treatments, we must first understand more clearly the mechanisms underlying their suppression in the TME.

PGE₂ is an inflammatory mediator. Although PGE₂ promotes cancer progression in the TME, it also drives and regulates acute inflammation necessary to heal tissue damage under normal physiological conditions [16]. In the final stages of wound healing, PGE₂ can act to resolve acute inflammation by inhibiting the synthesis of IL-2 which leads to suppression of NK cells and cytotoxic T cells [16].

PGE₂ has been found to directly suppress NK cell function [6, 7, 17] by signaling through both prostaglandin receptor 2 (EP2) and receptor 4 (EP4) [6, 17, 18]. However, it is unclear precisely how PGE₂ influences NK cell tumor-restraining functions. For example, it is well-established that there are several discrete steps to immune synapse formation leading to cytolysis but little is known about how PGE₂ impacts the dynamics of synapse formation. Likewise, serial killing by NK cells is an important component of their overall response, and again the effect of PGE₂ on this has not been studied extensively. Here, we show that PGE₂ affects several but specific features of the antitumoral NK cell immune

response: from initial migration into the tumor, the dynamics of how NK cells and cancer cells interact, the production of IFN- γ , and eventual cancer cell killing.

Results

PGE₂ reduces the expression and function of multiple NK cell activating receptors

To investigate the effects of PGE₂ on NK cell cytotoxicity, degranulation of peripheral blood NK cells was measured in response to the transformed B cell line, 721.221 (hereafter referred to as 221) and the chronic myelogenous leukemia K562 cell line. These cancer cell lines, along with Burkitt's lymphoma Daudi cells, used as targets in later experiments, express little or no HLA class I protein and are susceptible to NK cell-mediated cytotoxicity [19–21]. They also do not express the gene encoding COX-2 (PTGS2) [22] or produce PGE₂ (Supporting information Fig. S1A). Thus, synthetic PGE₂ could be dosed in a controlled manner. Human NK cells were rested for 6 days with low-dose IL-2 and incubated with or without PGE₂ for 24 h, before co-incubation with target cells at a 1:1 effector to target ratio (E:T) for 4 h. The PGE₂ dose was selected based on previous studies [17, 23] and titrations shown in Supporting information Fig. S1B. PGE₂ treatment significantly reduced NK cell degranulation, marked by surface expression of CD107a, in response to 221 or K562 target cells, by $15.0 \pm 5.9\%$ and $26.4 \pm 14.9\%$, respectively (Fig. 1A, B). Importantly, PGE₂ did not affect NK cell viability determined by staining with a dead cell marker (Fig. 1C), indicating that the reduction in NK cell cytotoxicity was not a result of PGE₂-inducing NK cell death.

NK cells express a diverse repertoire of germline-encoded activating and inhibitory receptors that recognize altered expression of proteins on target cells and control cytolysis [3]. We therefore tested if expression of these receptors is affected by PGE₂. For this, NK cells were treated with PGE₂ for 0, 2, 5, or 24 h prior to phenotypic analysis via flow cytometry. There was a gradual time-dependent decrease in NK cell surface expression of the activating receptors NKG2D, NKp30, and NKp44 following PGE₂ treatment (Fig. 1D, Supporting information Fig. S2A). In contrast, NK cell surface expression of the activating receptor NKp46, Fc receptor CD16, and inhibitory receptors KIR2DL1, KIR2DL2/L3, NKG2A, and TIGIT were unchanged by PGE₂ (Fig. 1D, Supporting information Fig. S2B). The analysis also suggested that TRAIL was downregulated by PGE₂. However, minimal expression could be detected at the NK cell surface, so this is unlikely to impact killing in our system (Supporting information Fig. S2C, D). Moreover, NK cell killing on the timescale studied here is predominantly mediated by granule secretion [24]. Overall, PGE₂ has differential effects on NK cell receptor expression, affecting some activating receptors but not others.

To investigate if PGE₂ has different effects on NK cell cytotoxic function depending on the specific receptor ligated for stimulation, we made use of P815 mouse mastocytoma cells which express Fc γ receptors on their surface. P815 cells can bind the Fc portion of mouse IgG antibodies, which through their

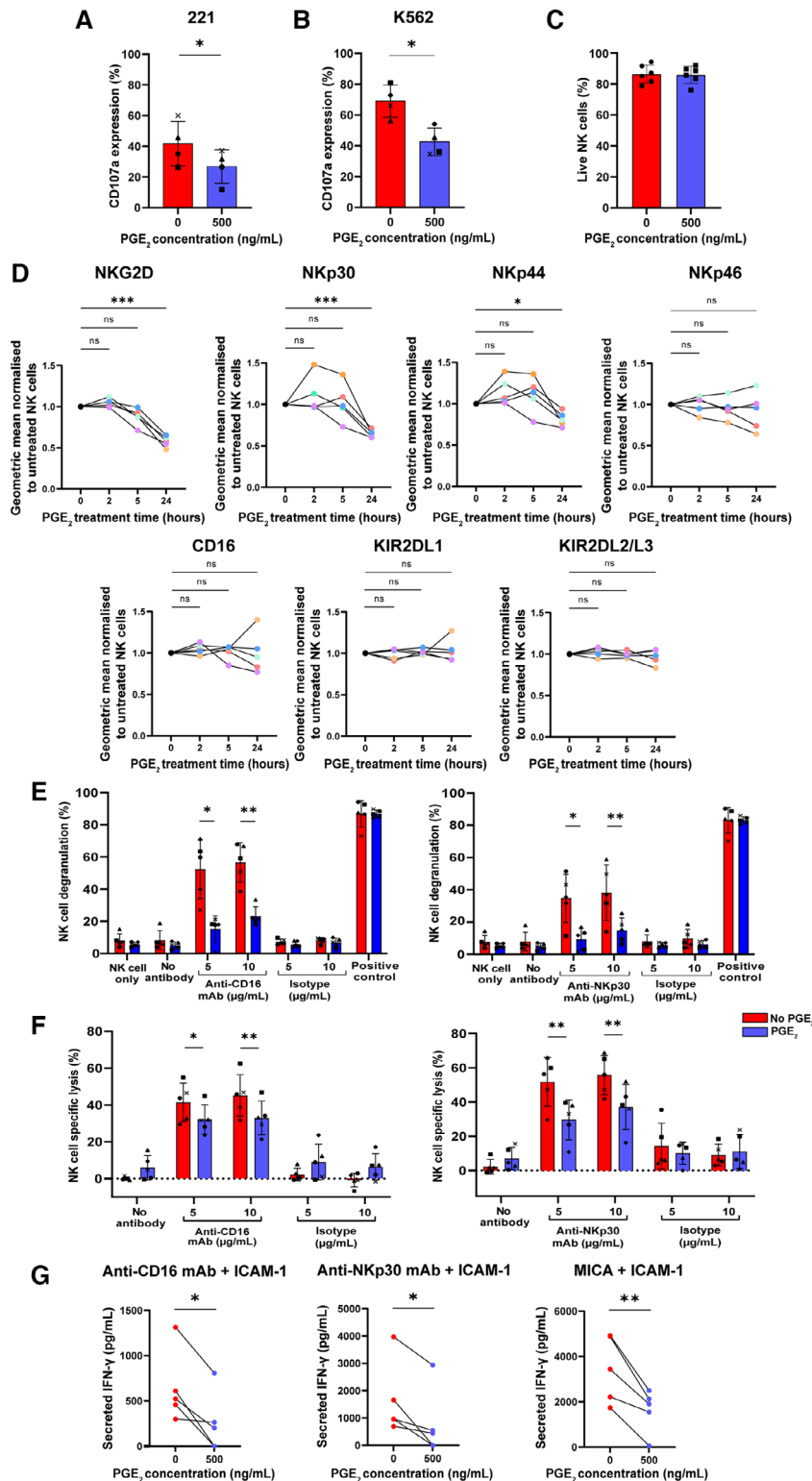


Figure 1. PGE₂ reduces the expression and function of multiple NK cell-activating receptors. (A, B) NK cells were incubated with or without PGE₂ for 24 h and subsequently co-incubated with 221 (A) or K562 (B) target cells for 4 h at a 1:1 ratio. The percentage of cells with surface CD107a expression was quantified by flow cytometry as a measure of NK cell degranulation, n = 4 independent donors. (C) NK cell viability was assessed by staining with a dead cell marker, n = 6 independent donors. (D) NK cells were incubated with 500 ng/mL PGE₂ for 0, 2, 5, or 24 h, and the expression of surface activating and inhibitory receptors was determined via flow cytometry. Graphs show geometric means for receptor expression on NK cells normalized to untreated NK cells, n = 5 independent donors. (E, F) P815 target cells were opsonized for 45 min with mAb (as indicated) before being co-incubated with NK cells for 4 h at a 1:1 ratio. (E) Percentage CD107a expression was quantified by flow cytometry as a measure of NK cell degranulation, n = 5 independent donors. Phorbol-12-myristate 13 acetate (PMA) and ionomycin were used as positive control. (F) NK cell-specific lysis of targets was measured by staining with Annexin V and propidium iodide, n = 5 independent donors. (G) PGE₂-treated or untreated NK cells were incubated overnight in wells coated with MICA, anti-NKp30 mAb, or anti-CD16 mAb, with ICAM-1 or ICAM-1 alone. Cell supernatants were then collected for analysis of IFN-γ secretion by ELISA, n = 5 independent donors, and experiments. Mean ± SD are indicated. *P < 0.05, **P < 0.01, ***P < 0.001 calculated by paired t-tests.

antigen-binding fragment can recognize NK cell activating receptors and stimulate cytotoxicity, a process known as redirected lysis [25]. We opsonized P815 cells with various concentrations of anti-CD16 or anti-NKp30 mAbs (Supporting information Fig. S3B). These were selected for comparison because CD16 expres-

sion was unaffected by PGE₂ whilst NKp30 expression was down-regulated (Fig. 1D). Opsonizing P815 cells with 5 µg/mL anti-CD16 mAb induced degranulation in 52.3 ± 18.3% untreated NK cells whereas PGE₂ reduced this to 15.2 ± 8.2% (Fig. 1E). A similar effect was observed when P815 cells were opsonized

with 5 $\mu\text{g}/\text{mL}$ anti-NKp30 mAb. In that case, $36.3 \pm 15.6\%$ of untreated NK cells degranulated whereas PGE₂ treatment reduced this to $9.7 \pm 7.1\%$ of cells (Fig. 1E). We also assessed the direct lysis of opsonized P815 cells after 4 h co-incubation with NK cells, by staining with Annexin V, a marker of apoptosis, and PI, indicative of membrane permeability [26]. PGE₂ significantly inhibited NK cell-specific lysis of P815 opsonized with either anti-CD16 or anti-NKp30 mAbs (Fig. 1F). IFN- γ secretion by NK cells was likewise inhibited by PGE₂, regardless of whether the cells were stimulated via the CD16, NKp30, or NKG2D (MICA ligand) activating pathways (Fig. 1G). Thus, although PGE₂ had differential effects on NK cell surface expression of CD16 and NKp30, it could nevertheless inhibit NK cell killing, degranulation, and IFN- γ production stimulated via either of these receptors. This implies that PGE₂ inhibits NK cell activating receptor signaling via a mechanism additional to the downregulation of receptor expression.

Transcriptome profiling reveals that PGE₂ modulates NK cell chemotaxis pathways

To further explore the action of PGE₂ on NK cells we next investigated its effects at the transcriptional level. Bulk RNA sequencing of NK cells from three individual donors revealed a number of genes differentially expressed with PGE₂ treatment. This included the chemokine receptor *CXCR3* and effector molecule *GZMK* which were downregulated and the chemokine receptor *CXCR4* and inhibitory receptor *CTLA4* which were found to be upregulated upon PGE₂ treatment (Fig. 2A, B). Additionally, the effects on NK cell activating and inhibitory receptor expression observed in Fig. 1D were replicated at the transcriptional level, with the exception of *KLRK1*, encoding NKG2D, which was expressed at low levels in these donors. To further characterize the biological processes underlying the transcriptional changes induced by PGE₂, we performed gene set enrichment analysis using the MSigDB biological processes ontology gene subset [27, 28]. Several pathways were found to be altered in NK cells upon culture with PGE₂. This included downregulation of inflammatory and immune responses, response to TNF, cytokine-mediated signaling, regulation of the ERK cascade, and chemotaxis (Fig. 2C). We chose to explore two key chemokine receptor hits, *CXCR3*, which was downregulated by PGE₂ and *CXCR4* which was upregulated (Fig. 2D, E). We verified these hits by flow cytometry and found that *CXCR3* expression was significantly decreased at the NK cell surface, whilst *CXCR4* expression was significantly increased upon PGE₂ treatment (Fig. 2F–H). These changes in protein expression could be observed as both changes in geometric mean fluorescence and changes in the percentage of positive cells (Fig. 2G, H).

PGE₂ decreases NK cell migration to CXCL10 but increases NK cell migration to CXCL12

Given that the change in chemokine receptor expression could be observed at both the transcriptional and translational level,

we hypothesized that PGE₂ would impair NK cell migration toward the chemokine CXCL10, a ligand for CXCR3, but increase migration toward the CXCR4-ligand, CXCL12. Using transwell assays, we observed a dose-dependent increase in specific NK cell migration toward both CXCL10 and CXCL12. Consistent with the changes in CXCR3 and CXCR4 expression induced by PGE₂, PGE₂ treatment decreased specific NK cell migration toward CXCL10 but increased specific migration toward CXCL12 (Fig. 3A, B). We used this knowledge to explore the effects of PGE₂ on NK cell migration more thoroughly using the ibidi μ -slide; a microfluidics slide that maintains stable chemotactic gradients for analysis of real-time chemotaxis (Supporting information Videos S1 and S2). We analyzed parameters describing single-cell movement including length of NK cell migration, forward migration index (the efficiency of forward migration of cells; FMI), average velocity, and directness of migration (straightness of the NK cell trajectory path). NK cells exhibited random movement in the absence of chemokines, with no chemotaxis effect observed (Fig. 3C–L). When NK cells were exposed to a stable gradient of 10 nM CXCL10, they migrated efficiently toward the chemokine source (Fig. 3C). PGE₂ treatment impaired this chemotactic response. NK cells exhibited a decreased forward migration index, migrated a shorter distance, at a slower speed, and were less direct in their trajectory path compared with untreated cells (Fig. 3E–H). The reverse was true for NK cells exposed to a stable gradient of 100 nM CXCL12 (Fig. 3D). PGE₂-treated NK cells migrated efficiently toward CXCL12, exhibiting a greater FMI, distance migrated, migration velocity, and directness of migration compared with untreated NK cells (Fig. 3I–L). Thus, PGE₂ alters NK cell migration by reducing CXCR3- and increasing CXCR4-mediated chemotaxis.

PGE₂ reduces the frequency and speed of NK cell killing

To better understand how PGE₂ impairs NK cell cytotoxicity we used live-cell time-lapse microscopy to observe NK cell ligation and killing of cancer targets in the presence or absence of PGE₂, to mimic its presence or absence in the TME (Fig. 4A). To reflect immune cells being outnumbered by cancerous cells in the TME, 221 or Daudi cancer cell lines were co-incubated with NK cells at an E:T ratio of 1:4 (Fig. 4B). Cells were imaged in fibronectin-coated wells in the presence of To-Pro-3 dye which indicated cell death by its entry into the target cell (Fig. 4B). In some cases, target cells were killed rapidly, and NK cells went on to sequentially kill other targets in close proximity (Supporting information Video S3). In contrast, other NK cells took significantly longer time to kill the target after conjugation had taken place (Supporting information Video S4). In some instances, NK cells would fail to kill the target and detach (Supporting information Video S5). In the example shown in Fig. 4B, an NK cell encountered the first target cell, the second target cell 6 min later, and the third target cell 36 min after that.

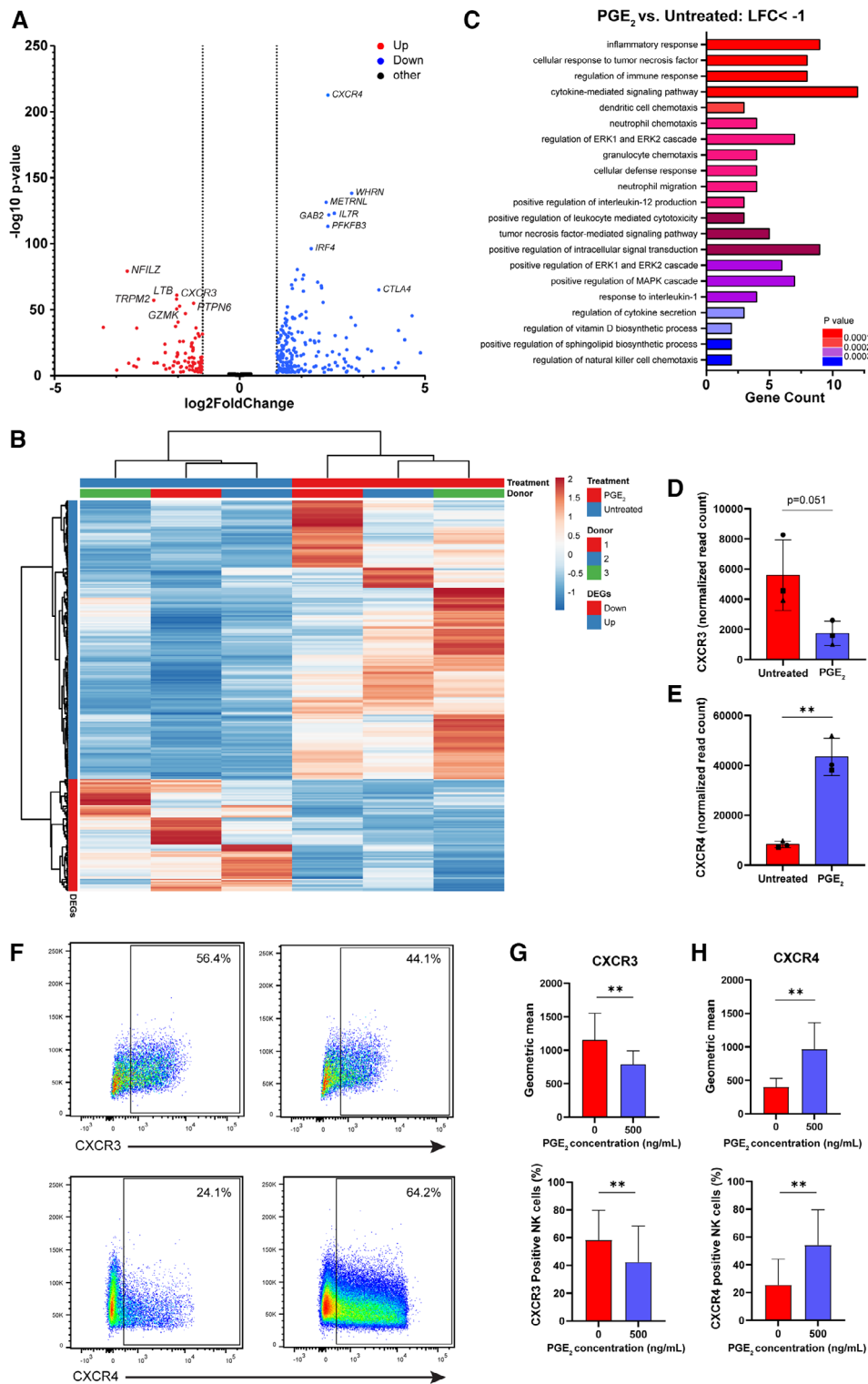


Figure 2. RNA sequencing reveals modulation of NK cell chemotaxis pathways by PGE₂. (A–E) RNA was extracted from untreated or PGE₂-treated (500 ng/mL) NK cells and analyzed by bulk RNA sequencing, *n* = 3 independent donors. (A) Volcano plot showing differentially expressed genes (*P* < 0.1 and a log fold change < 1 or > 1). (B) Hierarchical clustering and heatmap representation of top differentially expressed genes between untreated (blue) and PGE₂-treated (red) NK cells and independent donors. Both rows and columns are clustered using correlation distance and average linkage. (C) Bar graph showing the top significantly downregulated biological processes (gene ontology biological processes subset) in NK cells upon PGE₂ treatment, identified by EnrichR Gene set enrichment analysis. Gene count is the number of genes contributing to the enrichment. (D, E) Normalized gene read counts (by DESeq2) of CXCR3 (D) and CXCR4 (E) for untreated and PGE₂-treated NK cells. (F, G, H) Expression of CXCR3 and CXCR4 at the NK cell surface, determined by flow cytometry, *n* = 7 independent donors. Mean ± SD are indicated. ***P* < 0.01 calculated by paired *t*-tests.

Analysis of killing kinetics revealed that the probability of an NK cell-target cell conjugation resulting in a kill was significantly reduced in the presence of PGE₂ for both 221 and Daudi targets (Fig. 4C, D). In control co-cultures, without PGE₂, 74.7 ± 8.2 % of conjugations between an NK cell and a 221-target cell resulted in a kill, whereas in the presence of 100 ng/mL PGE₂,

this decreased to 49.3 ± 12.4% and to 45.5 ± 9.7% with 500 ng/mL PGE₂ (Fig. 4C). This same effect was also apparent for the killing of Daudi cells following conjugation, with the likelihood of a target cell conjugation resulting in a kill reducing from 61.7 ± 17.1% to 34.4 ± 21.2% in the presence of 500 ng/mL PGE₂ (Fig. 4D).

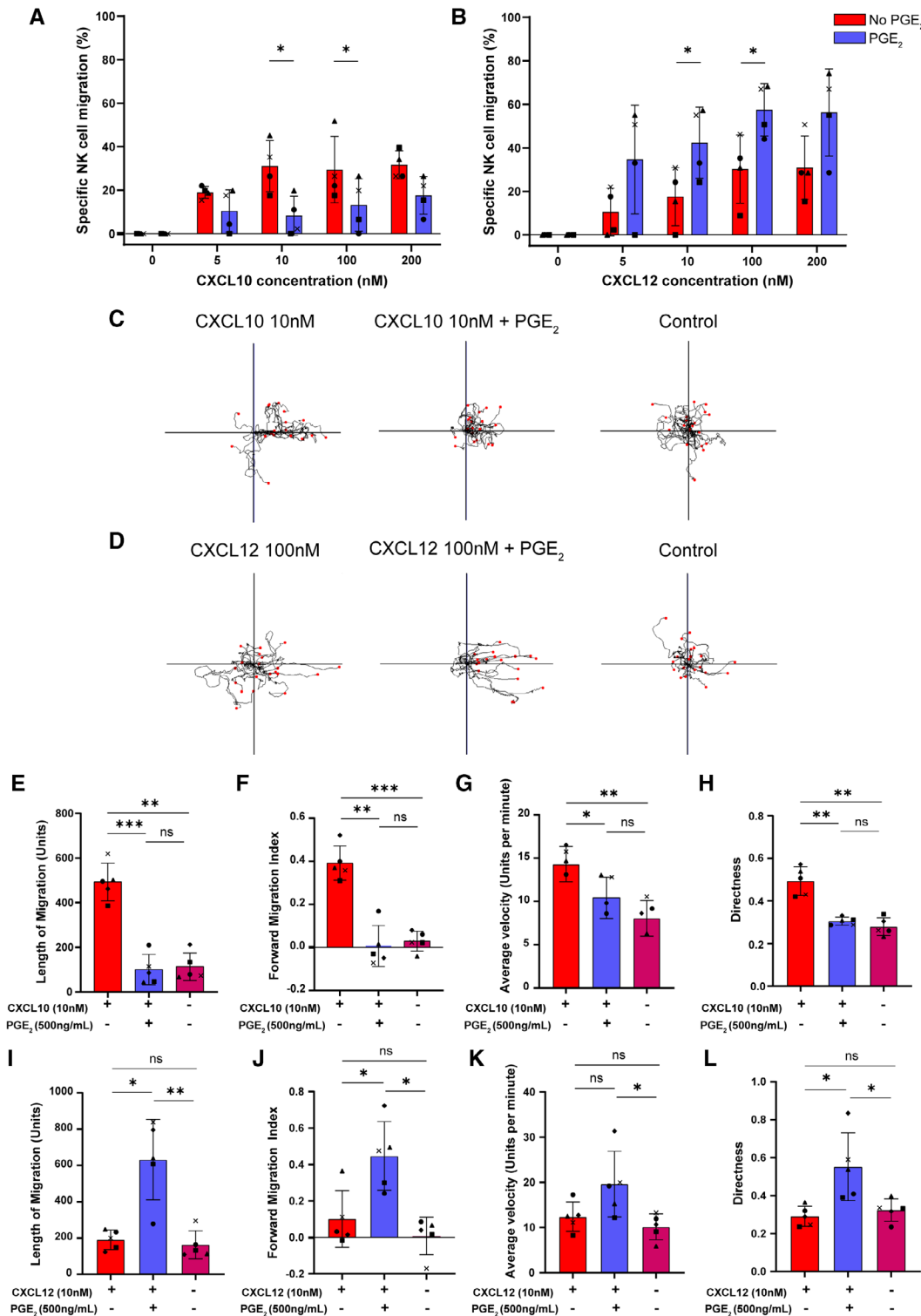


Figure 3. PGE₂ decreases NK cell migration toward CXCL10 but increases NK cell migration toward CXCL12. (A, B) Untreated or PGE₂-treated (500 ng/mL) NK cells were assessed for their chemotactic response to increasing concentrations of CXCL10 (A) or CXCL12 (B) in transwells, over 2.5 h. Specific NK cell migration was quantified as a percentage of the total cells applied to the filter, $n = 4$ independent donors. (C–L) NK cells were imaged in μ -slides (ibidi) in the presence of a CXCL10 (C, E–H) or CXCL12 (D, I–L) gradient for analysis of chemotaxis by widefield time-lapse microscopy using a $10\times/0.3$ NA objective. Images were acquired every 2 min for 4 h. (C) Representative cell trajectory plots for untreated and PGE₂ treated NK cells in the presence of a 10 nM CXCL10 gradient. (D) Representative cell trajectory plots for untreated and PGE₂ treated NK cells in the presence of a 100 nM CXCL12 gradient. Control in (C) and (D) is NK cells in the presence of no chemokine. Axes are $\pm 1591 \mu\text{m}$. (E, I) Length of NK cell migration (based on center of mass), (F, J) NK cell forward migration index (FMI), (G, K) average NK cell velocity, and (H, L) directness of NK cell migration were quantified, $n = 5$ independent donors. Mean \pm SD are indicated. * $P < 0.05$, ** $P < 0.01$, *** $P < 0.001$ calculated by paired t -tests.

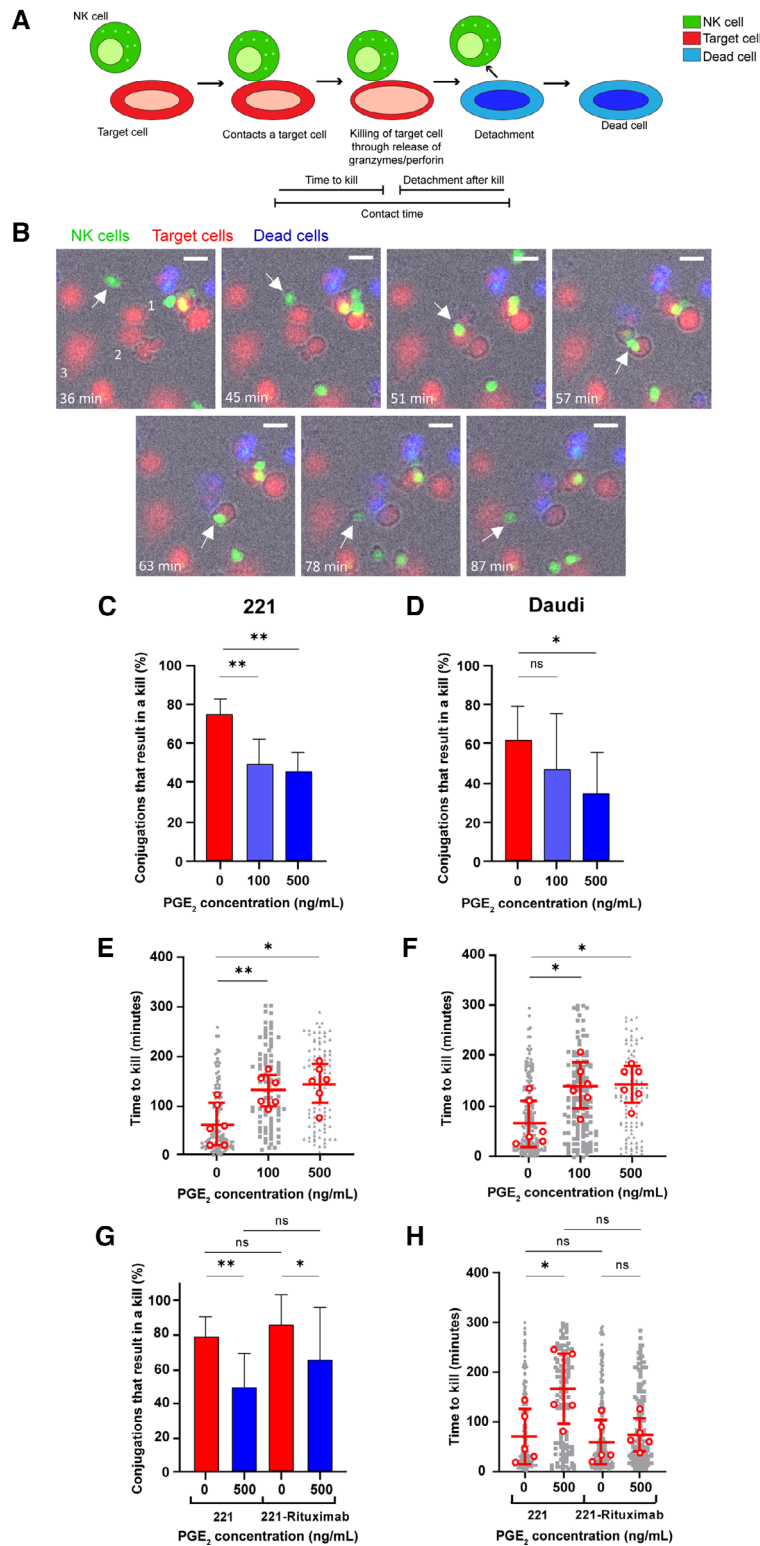


Figure 4. PGE₂ reduces the frequency and speed of NK cell killing. NK cells were co-incubated with 221, Rituximab-opsized 221 or Daudi target cells at E:T 1:4 on slides, in the presence or absence of PGE₂ and imaged via widefield time-lapse microscopy using a 20x/0.75 NA objective. Images were captured every 3 min for 5 h. (A) Schematic illustration of an NK cell-target cell interaction that results in a kill followed by detachment. (B) Example time course from one enlarged region of a single field of view, in fluorescence overlaid onto a bright field, with time indicated. NK cells are shown in green, target cells in red, and dead cells in blue. The example sequence shows an NK cell (indicated with an arrow) contacting 3 221 targets sequentially as indicated [1–3]. The NK cell encountered the first target cell at 45 min, the second target cell at 51 min, and the third target cell at 87 min, scale bar = 20 μm. (C, D) The percentage of NK cell-target cell conjugations that result in a kill for 221 (C) and Daudi (D) targets, in the presence or absence of PGE₂, n = 6 independent donors. (E, F) Analysis of time taken for an NK cell to kill a 221 (E) or Daudi (F) target cell after conjugation in the presence or absence of PGE₂, n = 6 independent donors. Each dot represents one individual cell and each open circle represents the median of the individual donors. (G) The percentage of NK cell-target cell conjugations that result in a kill for 221 and Rituximab-opsized 221 targets, in the presence or absence of PGE₂, n = 5 independent donors. (H) Analysis of time taken for an NK cell to kill a 221 or Rituximab-opsized 221 target cell after conjugation, in the presence or absence of PGE₂, n = 5 independent donors. Each dot represents one individual cell and each open circle represents the median of the individual donors. Mean ± SD are indicated. *P < 0.05, **P < 0.01 calculated by paired t-tests.

Killing of target cells is a binary event, a singular outcome of the balance between activating signals and inhibitory signals. However, the time taken to kill was also increased in the presence of PGE₂, for both 221 and Daudi target cells. Time to kill increased by 68 ± 36 min in the presence of

100 ng/mL PGE₂ and by 81 ± 68 min in the presence of 500 ng/mL PGE₂, for 221 target cells (Fig. 4E). For Daudi target cells, time to kill increased by 75 ± 64 min with 100 ng/mL PGE₂ (Fig. 4F). There is considerable variability in the time it takes for individual NK cells to kill target cells but

on average PGE₂ significantly increased NK cell killing time (Fig. 4E, F).

Interestingly, the effects of PGE₂ on time to kill could be rescued with the addition of another stimulating pathway, triggered by Rituximab. Rituximab is a monoclonal antibody that targets CD20, a surface transmembrane protein expressed on B cells, to induce antibody-dependent cell-mediated cytotoxicity via CD16 [29]. 221 cells were opsonized with Rituximab prior to co-incubation with NK cells. For Rituximab-opsonized 221 cells, the likelihood of an NK cell conjugation resulting in a kill was still reduced by PGE₂, but to a lesser extent than for non-opsonized 221 target cells (Fig. 4G). This was also seen in assays using flow cytometry, in which the presence of Rituximab significantly increased specific lysis by both untreated and PGE₂-treated NK cells. However, in the presence of Rituximab, specific lysis was still decreased when NK cells were exposed to PGE₂ (Supporting information Fig. S4). The increase in time to kill of 97 ± 77 min induced by PGE₂ for 221 targets, however, was completely abolished for Rituximab-opsonized 221 (Fig. 4H). Thus, PGE₂ can inhibit NK cell killing capacity and slow down the ability of NK cells to kill following initial target cell conjugation. Providing an additional level of activation via Rituximab can augment or rescue NK cell killing time and partially rescue overall killing.

PGE₂ inhibits NK cell MTOC polarization and ERK1/2 phosphorylation

To investigate the mechanism underlying the changes in NK cell killing kinetics, we next tested the effect of PGE₂ on the discrete steps required for efficient NK-cell cytotoxicity: re-organization of the actin cytoskeleton, polarization of the microtubule organizing center (MTOC) and release of lytic granules [30]. Characteristic of an NK cell forming an activating immune synapse with a target cell, F-actin accumulates in a dense ring, presumed to facilitate tight adhesion between cells [31–36]. To measure actin ring formation, PGE₂-treated or untreated NK cells were activated on coated slides before being fixed and stained with phalloidin to mark F-actin (Fig. 5A). PGE₂ had no effect on NK cell actin ring formation stimulated via the NKG2D, NKp30, or CD16 activating pathways (Fig. 5B).

Following actin reorganization, polarization of the MTOC is a critical step in NK cell cytotoxicity. It is responsible for organizing the microtubules that subsequently transport lytic granules to the immune synapse for secretion [37]. The ability of NK cells to polarize in response to PGE₂-treated cells was determined by imaging NK cell–cancer cell conjugates. To visualize the MTOC, cells were stained for pericentrin, an MTOC component (Fig. 5C, Supporting information Fig. S5). MTOC polarization was then quantified by measuring the distance of the MTOC from the immune synapse. PGE₂-treated NK cells exhibited impaired MTOC polarization compared with untreated cells, indicated by an increased distance of the MTOC from the immune synapse (Fig. 5D). At 10 min, the relative distance of the MTOC from the immune synapse was 0.31 ± 0.17 compared with 0.22 ± 0.14 for

untreated NK cells (Fig. 5D). At 20 min the effect of PGE₂ was greater, with the MTOC relative distance 0.37 ± 0.23 , compared with 0.25 ± 0.19 (Fig. 5D). At 40 min, however, all NK cells were polarized to a similar extent (Fig. 5D). Therefore, PGE₂ delays the ability of the NK cell MTOC to polarize toward the immune synapse.

In NK cells, the ERK pathway is known to regulate granule polarization and reorientation of the MTOC [38]. Thus, we tested if PGE₂ affects the levels of phosphorylated ERK1/2. For this, NK cells were challenged with 221 target cells and intracellular phosphorylated ERK1/2 was measured by flow cytometry. Prior to activation, PGE₂-treated NK cells expressed slightly lower levels of phosphorylated ERK1/2 compared with untreated NK cells (Fig. 5E). However, upon activation with 221 target cells phosphorylated ERK1/2 levels increased more than two-fold and were significantly lower in NK cells that had been exposed to PGE₂ (Fig. 5E). Additionally, the integrin LFA-1 expressed on NK cells is known to play a central role in immune synapse assembly and granule secretion. Binding of NK cell LFA-1 to target cell ICAM-1 mediates adhesion and is important for polarization of NK cell cytolytic granules [39–42]. We observed that PGE₂ treatment reduced NK cell expression of LFA-1 and ICAM-1 at both the transcriptional and translational level, to some extent (Fig. 5F, Supporting information Fig. S6A). This downregulation did not significantly affect the ability of NK cells to adhere to and form conjugates with 221 target cells (Supporting information Fig. S6B). It is possible that reduced LFA-1 signaling may contribute to the delay in MTOC polarization induced by PGE₂. In contrast, PGE₂ did not affect downstream signaling of NK cell activation, as evident by imaging the recruitment of phosphorylated signaling proteins CD3 ζ or Zap-70 (Supporting information Fig. S7). PGE₂ therefore does not interfere with membrane-proximal early activating signals, or specifically CD3 ζ or Zap-70 phosphorylation.

Finally, to achieve a target cell kill, NK cells must release lytic granules which typically contain the pore-forming protein perforin, and the serine protease granzyme B which induces target cell apoptosis [30]. To investigate the effects of PGE₂ on the release of lytic granules a technique termed “shadow imaging” was used, an imaging method allowing assessment of secretions from individual NK cells [43–45]. PGE₂-treated or untreated NK cells were incubated for 1 h on slides coated with MICA, anti-NKp30 mAb, or anti-CD16 mAb, with ICAM-1, or ICAM-1 alone. Slides were then stained for 1 min with anti-ICAM-1 mAb, cells were detached to leave “shadows” and slides stained for perforin (Fig. 5G, Supporting information Fig. S8). Intensity of secreted perforin within shadows was then quantified. PGE₂ was found to have no effect on NK cell perforin secretion when cells were activated with MICA, anti-CD16, or anti-NKp30 mAb (Fig. 5H). We additionally assessed NK cell expression of granzyme B and perforin by intracellular flow cytometry and RNA sequencing analysis. Surprisingly, PGE₂ treatment increased NK cell expression of both granzyme B and perforin to some extent, even though the quantity of perforin secreted from individual NK cells was not perturbed (Supporting information Fig. S9).

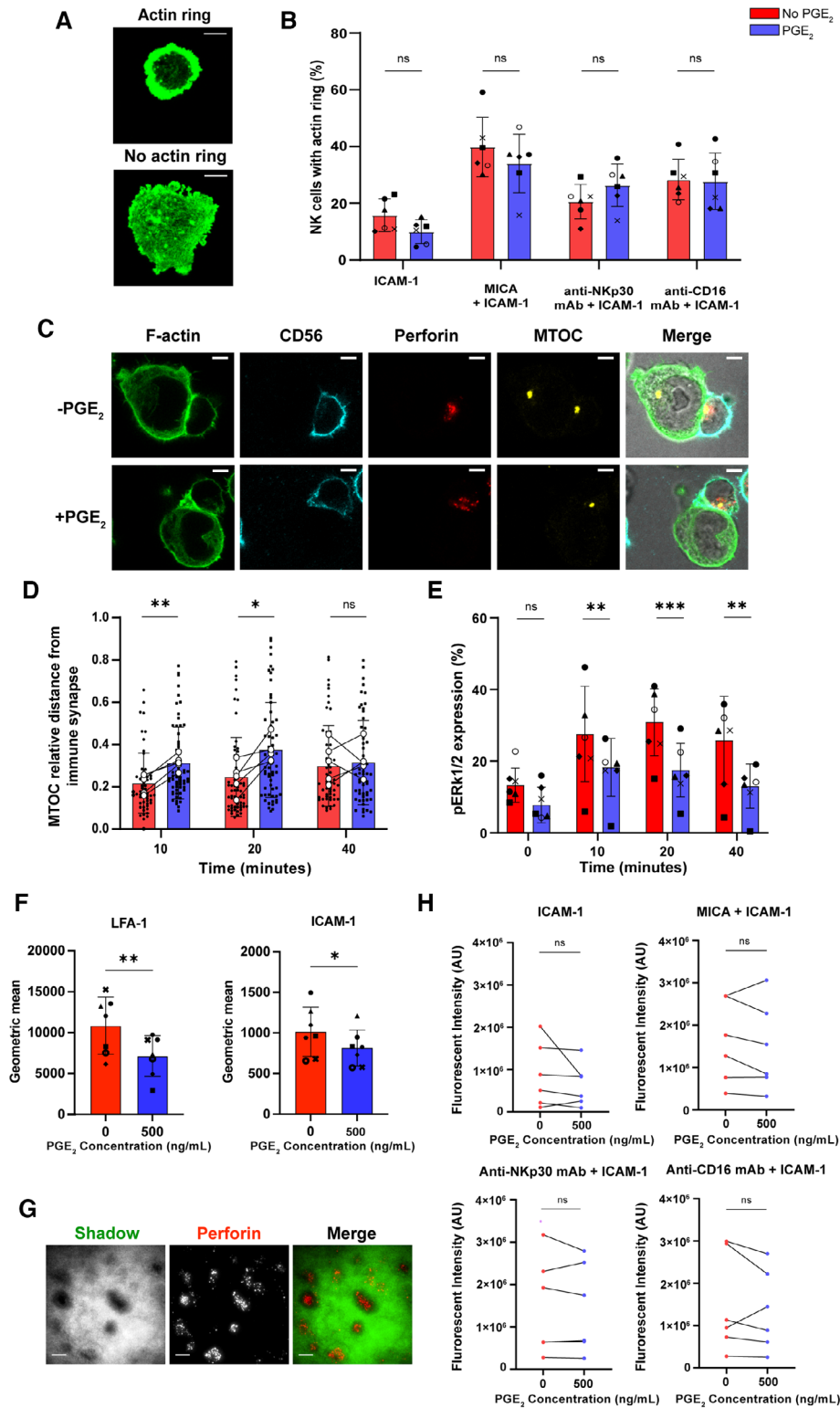


Figure 5. PGE₂ inhibits NK cell MTOC polarization and ERK1/2 phosphorylation. (A, B) PGE₂-treated or untreated NK cells were incubated for 5 min on slides coated with MICA, anti-NKp30 mAb, or anti-CD16 mAb, with ICAM-1 or ICAM-1 alone. Cells were then fixed, stained for F-actin, and imaged by confocal microscopy, using a 100×/1.4 NA oil immersion objective. (A) Representative images showing an NK cell actin ring versus no actin ring upon stimulation with MICA and ICAM-1, scale bars = 5 μm. (B) Stimulated NK cells were stratified according to their F-actin distribution, n = 6 independent donors. (C, D) PGE₂-treated or untreated NK cells were incubated with 221 target cells for 10, 20, or 40 min. Conjugates were then fixed, stained, and imaged by confocal microscopy using a 63×/1.40 NA oil immersion objective. (C) Representative images of NK cell-221 target cell conjugates stained with AF488-labeled phalloidin, BV421 anti-CD56 mAb, AF647 anti-perforin, and anti-pericentriolar mAb followed by AF568-labeled goat anti-rabbit secondary mAb. Scale bars = 5 μm. (D) Relative distance of the MTOC from the immune synapse. Polarization of the MTOC was quantified by dividing the distance of the interface to the MTOC by the length of the NK cell. Each dot represents one individual cell and each white circle represents the mean of n = 5 individual donors. (E) Phosphorylated ERK1/2 levels in untreated or PGE₂-treated NK cells upon activation with 221 target cells for 0, 10, 20, or 40 min, determined by intracellular staining and flow cytometry. n = 6 independent donors. (F) Expression of LFA-1 and ICAM-1 at the NK cell surface, determined by flow cytometry, n = 7 independent donors. (G, H) PGE₂-treated or untreated NK cells were incubated for 1 h on slides coated with MICA, anti-NKp30 mAb, or anti-CD16 mAb, with ICAM-1 or ICAM-1 alone. Slides were then stained for 1 min with anti-ICAM-1 mAb, cells were detached to leave “shadows” and slides were stained for perforin. Slides were imaged by TIRF microscopy using an Apo TIRF 100×/1.49 NA oil objective. (G) Representative images of shadows formed by NK cells activated with anti-NKp30 mAb and ICAM-1. Scale bars = 10 μm. (H) Intensity of secreted perforin per cell for NK cells activated with MICA, anti-CD16 mAb, anti-NKp30 mAb, with ICAM-1 or ICAM-1 alone. Each dot represents the mean of n = 6 independent donors. Mean ± SD are indicated. *P < 0.05, **P < 0.01, ***P < 0.001 calculated by paired t-tests.

Interestingly, although PGE₂ impairs NK cell degranulation in response to target cells (Fig. 1A, B, and E) when NK cells are activated on slides it has no effect on the quantity of secreted perforin. This may be a consequence of the complexity of a cell-cell interaction versus the reductionist method of stimula-

tion on antibody-coated slides. For example, the effects of PGE₂ might be less evident if a very high number of activating signals are triggered as likely to be the case with antibody-coated slides. Moreover, there is a precedence for the stiffness of the surface used for immune-cell activation being important [46].

Glass in particular, can affect functional outcomes significantly [47].

We conclude that a delay in NK cell polarization may explain the delay in NK cell killing, induced by PGE₂. Moreover, the delay in NK cell polarization induced by PGE₂ and the reduction in NK cell killing of target cells is likely a result of disrupted signaling pathways, such as the observed reductions in ERK1/2 phosphorylation and LFA-1 expression.

Discussion

Tumor immune escape is a major factor contributing to cancer progression and the impaired success of cancer therapies [48]. COX-2, critical for production of the inflammatory mediator PGE₂, is often overexpressed by cancer cells [14] and the production of PGE₂ is one of the mechanisms by which they evade immunity [6, 48]. It has been shown that PGE₂ can directly act on NK cells to impair antitumor immune responses [17]. However, it is unclear precisely how PGE₂ influences NK cell tumor-restraining functions. Here, we show that PGE₂ affects NK cells in multiple ways.

Following PGE₂ treatment, NK cells exhibited altered expression of activating receptors, produced less IFN- γ , and showed a reduced ability to degranulate and kill cancer targets. The reduction in NK cell cytotoxicity induced by PGE₂ could not solely be attributed to decreased expression of an activating receptor since NK cell CD16 expression was unaffected by PGE₂, yet PGE₂ still inhibited NK cell cytotoxic function stimulated via CD16. PGE₂ also changed the dynamics of how NK cells and cancer cells interact. In the presence of PGE₂, NK cells were less likely to kill target cells and were slower in doing so. A delay in the ability of the NK cell MTOC to polarize may relate to the increased time it takes for NK cell killing in the presence of PGE₂. There is a precedence for impairment of NK cell polarization being a mechanism of tumor escape in MDA-MB-453 breast cancer cells [49]. However, this likely involves a process other than PGE₂ secretion as MDA-MB-453 cells do not express COX-2, according to data from the Cancer Cell Line Encyclopedia (Broad Institute). Interestingly, retargeting NK cells by chimeric antigen receptor (CAR) expression (targeting HER2) or antibody-induced antibody-dependent cell-mediated cytotoxicity restored NK cell polarization, increased ERK phosphorylation, and resulted in the killing of MDA-MB-453 cells [49]. Consistent with this, we observed that Rituximab, an anti-CD20 antibody, successfully used in the treatment of B-cell malignancies, was able to trigger efficient NK cell killing in the presence of PGE₂. It is possible that CAR-NK cells may also overcome PGE₂-mediated NK cell inhibition [50].

PGE₂ also disrupted NK cell migration. PGE₂-treated NK cells exhibited decreased migration to CXCL10, a chemokine that induces NK cell infiltration into tumors via CXCR3 but showed an increased ability to migrate to the CXCR4-ligand, CXCL12. Studies have also previously reported a negative correlation between tumor COX-2 expression and CXCL10 production, which can be overcome with COX inhibitors [51, 52]. The combination of

decreased CXCL10 production in the TME and decreased CXCR3 expression on NK cells would together signify a clear mechanism of immune evasion.

CXCR4 can also guide NK cells to tumors. NK cells engineered with a CAR to overexpress CXCR4 exhibited increased infiltration in a mouse model of glioblastoma [53]. This raises the question as to whether PGE₂ would induce a positive effect on NK cell infiltration through increased expression of CXCR4, which would seemingly oppose other effects of tumor-derived PGE₂ on NK cells. If that were true, the defects in NK cell killing kinetics caused by PGE₂ might be partially rescued by CXCL12. However, CXCR4 also helps to retain human NK cells within bone marrow [54, 55] and in mice, CXCR3-deficient NK cells have been shown to exhibit greater bone marrow homing [56]. Thus, the combination of increased expression of CXCR4 and decreased expression of CXCR3 on NK cells following exposure to PGE₂ may promote homing of NK cells to the bone marrow, rather than migration to the peripheral tissues, including the tumor and peripheral blood. Moreover, high concentrations of chemokines may actually repel cells expressing the cognate receptor as demonstrated for the CXCR4/CXCL12 axis in the context of T cells, in a murine melanoma model [57].

Analysis of the effects of PGE₂ on NK cells at the transcriptional level exposed a stark downregulation of key inflammatory and immune pathways in NK cells. We focused on the differentially expressed genes *CXCR3* and *CXCR4*, but there is scope to explore this dataset further. *CTLA4*, encoding the immune checkpoint protein CTLA-4, was found to be upregulated in NK cells upon PGE₂ treatment. Immune checkpoint inhibitors targeting CTLA-4 have gone on to induce durable responses in many cancer patients [58]. Primarily, however, the focus has been on targeting CTLA-4 in T cells. Our transcriptomic data suggests that anti-CTLA-4 treatments may additionally target NK cells in patients with COX-2-expressing tumors.

An important unresolved question is the duration of the effects of PGE₂ on NK cells. Fast et al. [59] investigated the effects of PGE₂ on gene expression of hematopoietic stem cells used for cord blood transplants. They observed that some genes were “transiently induced” whilst others were “permanently induced”. Thus, PGE₂ can induce both short- and long-term effects on human immune cells. Overall, it remains unclear whether the PGE₂-impaired functional state of NK cells described here can be reversed with specific treatments, or if PGE₂-treated NK cells recover their reactivity in time.

The COX-2/PGE₂/EP2-4 axis has emerged as a major conserved determinant by which numerous cancer types modulate their surrounding environment and avoid immune-mediated elimination [6]. NK cells have been identified as the primary target of PGE₂/EP2-4 signaling [6]. Thus, the prospect of exploiting NK cells to treat cancer has gained much attention. Given the plethora of effects of PGE₂ on NK cells, knockout of the PGE₂ receptors in CAR-NK cells could considerably increase their clinical benefit. Overall, our study reveals that there are multiple elements to the mechanism of action of PGE₂ on NK cells. Blocking the effects of tumor COX-2 expression will help us harness the cancer-inhibitory

function of the immune system for the development of more effective cancer treatments.

Materials and methods

Human primary NK cells

Peripheral blood leukocyte cones from healthy human donors were acquired from the National Blood Service under ethics license REC 05/Q0401/108 (University of Manchester). Peripheral blood mononuclear cells were purified by density gradient centrifugation using Ficoll-Paque (GE Healthcare; Life Sciences) and NK cells isolated by negative selection (NK cell isolation kit; Miltenyi Biotec). NK cells were cultured at 37°C and 5% CO₂ in DMEM medium (Sigma) containing 30% Ham's F-12, 10% human serum (Sigma), 1% nonessential amino acids (Sigma), 1 mM sodium pyruvate (Sigma), 2 mM L-glutamine, 50 U/mL penicillin–streptomycin, and 50 μM 2-mercaptoethanol (Gibco) (NK cell clone medium). NK cells were also supplemented with 200 U/mL IL-2 (Roche) and rested for 6 days prior to experiments. To investigate the effects of PGE₂, NK cell cultures were additionally supplemented with synthetic PGE₂ (Sigma) 24 h prior to experimentation unless otherwise stated.

Cell lines

The hematological cancer cell lines K562 (chronic myelogenous leukemia) and Daudi (Burkitt's lymphoma) and a transformed B-cell line 721.221 were used as NK cell susceptible targets and purchased from ATCC. Cells were cultured at 37°C and 5% CO₂ in RPMI-1640 (Sigma) medium with 2 mM L-glutamine (Gibco). P815 (mouse mastocytoma) cells were also used for re-directed lysis assays and were maintained in a DMEM medium (Sigma). All media were supplemented with 10% fetal calf serum (FCS; Sigma) and 50 U/mL penicillin–streptomycin (Sigma). All cell lines were routinely tested for mycoplasma infection using a PCR-based kit (PromoCell).

Flow cytometry

To assess the expression of cell surface receptors, cells were first washed in PBS and stained with Live/Dead fixable blue viability dye (Invitrogen) for 20 min at 4°C. Cells were washed with FACS buffer (PBS + 2% BSA + 0.01% Sodium azide) and blocked with 2% human serum (Sigma) in FACS buffer for 20 min at 4°C. Cells were then washed and stained for 30 min with mAb or the appropriate isotype-matched controls, in FACS buffer at 4°C. mAb used for cell surface staining were: BV711 anti-CD56 (HCD56), BV605 anti-NKG2D (1D11), BV421 anti-NKp46 (9E2), PerCP anti-CD16 (3G8), FITC anti-KIR2DL2/L3 (DX27), PE-Cy7 anti-KIR2DL1 (HP-MA4), PE anti-NKp30 (P30-15), APC/Cy7 anti-CD3 (SK7), APC anti-NKp44 (P44-8), FITC anti-NKG2A (S19004C),

PE-Cy7 anti-TIGIT (A15153G), PE anti-ICAM-1 (HA58), APC anti-TRAIL (RIK-2), PerCP anti-CD183 (G025H7; CXCR3), BV421 anti-CD184 (12G5; CXCR4) (all Biolegend), and BV605 anti-LFA-1 (G-25.2; BD Biosciences). Isotypes: mouse IgG1 (MOPC-21), mouse IgG2a (MOPC-173), mouse IgG2b (MPC-11) (all Biolegend). Finally, cells were fixed in 4% paraformaldehyde (PFA)/PBS for 20 min. For intracellular staining, cells were permeabilized (BD Phosflow Perm/Wash Buffer, BD Biosciences) according to the manufacturer's instructions and stained with AF647 anti-ERK1/2 mAb (20A; BD Biosciences), AF647 anti-Granzyme B (GB11; BD Biosciences), AF647 anti-perforin (dG9; Biolegend) or the isotype matched controls: mouse IgG1 (MOPC-21; BD Biosciences), mouse IgG2b (MPC-11; Biolegend) overnight at 4°C. Cells were analyzed on the BD FACSymphony (BD Biosciences). A total of 10,000 events were recorded within the live cell gate for each sample and data were analyzed using FlowJo v10 software. NK cells were identified as the CD56⁺ CD3⁻ population of live, single cells.

To assess degranulation, target cells were labeled with CellTrace Violet (CTV) cell proliferation dye (Invitrogen) and cultured with NK cells at a 1:1 ratio for 4 h at 37°C in complete RPMI-1640 medium containing GolgiStop and GolgiPlug (1/1000; BD Biosciences) and PE-Cy5 anti-CD107a mAb (H4A3; BD Biosciences) or isotype-matched control (IgG1; MOPC-21; BD Biosciences). Cells were washed with PBS and stained with a dead cell marker (Live/Dead Fixable Near IR; Invitrogen) for 20 min at 4°C. Cells were then blocked in 2% human serum (Sigma) for 20 min at 4°C, washed and stained with PE-Cy5 anti-CD107a mAb, BV711 anti-CD56 mAb, or isotype-matched controls for 30 min at 4°C. Cells were then fixed in 4% PFA/PBS for analysis by flow cytometry. NK cell degranulation was quantified by determining the percentage expression of surface CD107a.

Redirected lysis assays

P815 cells were used to perform redirected lysis assays. P815 cells were first opsonized by incubating for 45 min at 37°C with anti-CD16 mAb (3G8; BD Biosciences), anti-NKp30 mAb (MAB1849; R&D), or isotype-matched controls (IgG1; MOPC-21 and IgG2a; MOPC-173). Opsonized cells were then cultured with CTV-labeled (CellTrace Violet cell proliferation dye; Invitrogen) NK cells at a 1:1 ratio. To assess NK cell killing, cells were cultured for 4 h at 37°C and then washed by re-suspending in cold Annexin V binding buffer (25 mM CaCl₂, 1.4 M NaCl, 0.1 M HEPES). Cells were stained with APC Annexin V (Biolegend) for 15 min at room temperature and washed with Annexin V binding buffer. Finally, cells were stained with 1 μg/mL PI for immediate analysis by flow cytometry, using a BD FACS LSR Fortessa X-20 flow cytometer. The gating strategy is shown in Supporting information Fig. S3A. To calculate the percentage of specific lysis for each sample, the following calculation was used:

$$\begin{aligned} \text{NK cell specific lysis (\%)} \\ = \% \text{ Target cell lysis} - \% \text{ Spontaneous target cell lysis.} \end{aligned}$$

To assess NK cell degranulation, opsonized target cells and NK cells were cultured for 4 h at 37°C in the presence of GolgiStop and GolgiPlug (1/1000; BD Biosciences) and PE-Cy5 anti-CD107a mAb (H4A3; BD Biosciences) or an isotype-matched control (IgG1; MOPC-21; BD Biosciences). At hour 3 of incubation, Phorbol 12-myristate 13-acetate (10 ng/mL; Sigma) and ionomycin (1 µg/mL; Sigma) were added to one well to stimulate degranulation and act as a positive control. Cells were then stained as before for analysis of degranulation by flow cytometry.

Cytokine detection by enzyme-linked immunosorbent assay

Flat-bottom 96-well plates (Nunc MaxiSorp; Thermo Fisher Scientific) were coated with 0.01% Poly-L-Lysine (PLL; Sigma) for 15 min at 37°C before being washed three times with sterile filtered water and dried at 60°C for 1 h. Wells were then coated overnight at 4°C, with 50 µL/well ICAM-1 (2.5 µg/mL; Peak Proteins) alone or with 2.5 µg/mL MICA (Manchester Institute of Biotechnology), 5 µg/mL anti-NKp30 mAb (MAB1849; R&D), or 5 µg/mL anti-CD16 mAb (3G8; BD Biosciences) in PBS. After overnight incubation, wells were washed three times with PBS and 100,000 NK cells were added to each well in 100 µL clone medium. Cells were allowed to incubate overnight at 37°C and 5% CO₂. Cell supernatants were then collected and centrifuged for 5 min at 4°C to remove cell debris. Secretion of IFN-γ in cell supernatants was then quantified using an IFN-γ DuoSet ELISA kit (R&D Systems), according to the manufacturer's instructions.

Production of PGE₂ by human tumor cell lines was evaluated in culture supernatants, collected from cells grown to confluence, using a Prostaglandin E₂ monoclonal ELISA kit (Cayman Chemical). The assay was performed following the manufacturer's protocol.

Conjugate formation assay

To assess conjugate formation, NK cells and 221 target cells were stained with Calcein Red-Orange (Invitrogen) and CTV cell proliferation dye (Invitrogen) respectively. NK cells were incubated with 221 target cells at a 1:2 ratio for 10, 30, or 60 min at 37°C, before fixation with 2% PFA/PBS for 30 min at 4°C. Cells were then washed with FACS buffer and analyzed by flow cytometry. The percentage of NK cells conjugated was determined by quantifying the number of double-positive events as a proportion of the total number of NK cells.

Annexin V/propidium iodide staining for dead cells

221 cells were first opsonized with Rituximab (MedChemExpress) or an isotype-matched control (IgG1; SinoBiological) for 30 min at 37°C. Target cells were then cultured with CTV-labelled (Cell-Trace Violet cell proliferation dye; Invitrogen) NK cells at a 1:3 ratio. To assess NK cell killing, cells were co-cultured for 4 h at

37°C and then washed by resuspending in cold Annexin V binding buffer. Cells were stained with APC Annexin V (Biolegend) for 15 min at room temperature and washed with Annexin V binding buffer. Finally, cells were stained with 1 µg/mL PI for immediate analysis by flow cytometry, using a BD FACS LSR Fortessa X-20 flow cytometer. The percentage of specific lysis was calculated as before.

RNA sequencing

NK cells were resuspended in RLT buffer (RNeasy lysis buffer; Qiagen) containing 0.01% β-mercaptoethanol to lyse cells and stored at -80°C prior to RNA extraction. RNA was extracted from thawed samples using the RNeasy mini kit (Qiagen) as per the manufacturer's instructions. For bulk RNA sequencing, mRNA libraries were prepared using the Illumina stranded mRNA prep kit and sequenced using the Illumina NovaSeq6000. Data analysis was performed using the DESeq2 package. The DESeq2 model included the "treat" factor (PGE₂ and untreated groups) and the "donor" factor was included to control for sample pairing. Enrichment of molecular pathways (MSigDB) was evaluated for differentially expressed genes, with $P < 0.1$ and a log fold change < 1 or > 1 , using EnrichR software (maayanlab.cloud/Enrichr/). Volcano plots were generated using GraphPad Prism 9 (GraphPad Software) and heat maps using ClustVis software (biit.cs.ut.ee/clustvis/).

Transwell assay

Chemokine-induced cell migration was measured using 6.5 mm transwells with 5.0 µm pore polycarbonate membrane inserts (Corning). Various concentrations of recombinant human CXCL10 or CXCL12 (5, 10, 100, and 200 nM; R&D) were prepared from stock solutions, in NK cell clone medium and were added to the appropriate wells below the membrane. 250,000 NK cells were then added to the surface of each membrane and allowed to incubate for 2.5 h at 37°C. Membranes were then removed and the migrating NK cells were quantified by counting the cells in the lower wells using a hemocytometer. Specific NK cell migration was quantified as a percentage of the total cells applied to the filter.

Chemotaxis assay

Chemotaxis assays were performed using the µ-Slide Chemotaxis (ibidi) according to the manufacturer's protocol. NK cells were resuspended at 3×10^6 cells/mL in NK cell clone medium supplemented with 2% Geltrex (Thermo Scientific) and loaded into the migration chamber. Migration in response to the chemokines CXCL10 (10 nM; R&D) or CXCL12 (100 nM; R&D) was determined by imaging every 2 min, for 4 h at 37°C, using a Nikon Ti Eclipse Inverted microscope (Nikon) with a 10x/0.3 NA objective. Images were analyzed in ImageJ using the manual tracking

plug-in. Followed by analysis using the ibidi chemotaxis and migration tool (ibidi) to determine the length of migration (based on center of mass), FMI, velocity, and directness of migration.

Live time-lapse imaging

Live imaging of NK cell–cancer cell interactions was performed in chambered coverslips (ibidi) coated with 10 $\mu\text{g}/\text{mL}$ fibronectin (Sigma). NK cells were stained with 1 μM Calcein Red-Orange (Invitrogen) and target cells were stained with 1 μM Calcein Green (Invitrogen). To stain with calcein dyes, cells were first washed three times with 10 mL RPMI media and then incubated with dye solution (1 μM) in RPMI for 15 min at 37°C. For Rituximab opsonization, target cells were subsequently incubated with 10 $\mu\text{g}/\text{mL}$ Rituximab (MedChemExpress) for 45 min at 37°C. Labeled NK cells were then added to target cells at a 1:4 E:T ratio in RPMI media supplemented with 1 μL To-Pro-3 per well (Thermo Fisher), to discriminate dead cells, and PGE₂ at concentrations indicated in figures. Time-lapse imaging was performed at 37°C and 5% CO₂ for 5 h with an image acquired every 3 min. Imaging was performed using a Nikon Ti Eclipse Inverted microscope (Nikon) with a 20 \times /0.75 NA objective. Fluorescent and bright-field images were merged and cell–cell interactions were analyzed manually using ImageJ. A kill was defined as an interaction triggering entry of To-pro-3 into the target cell.

Conjugate imaging

NK cell–target cell conjugates were formed by incubating NK cells with cancer cells for 10, 20, or 40 min at 37°C before fixation with 4% PFA/PBS for 20 min at room temperature. Conjugates were permeabilized with 0.1% Triton X-100 (Sigma) for 10 min at room temperature, blocked with 3% BSA in PBS for 1 h at room temperature, and stained with anti-pericentrin mAb (ab4448; Abcam) in blocking buffer for 2 h at 4°C. Conjugates were then washed with PBS and stained for 1 h at room temperature with AF568-labeled goat anti-rabbit secondary mAb (Invitrogen), AF647 anti-perforin mAb (dG9; Biolegend), AF488-labeled phalloidin (Invitrogen), and BV421 anti-CD56 mAb (HCD56; Biolegend). Finally, conjugates were washed again and transferred to PLL-coated (0.01%; Sigma) eight-chambered coverglass slides (Lab-Tek II; Nunc). Imaging was performed by confocal microscopy (SP8, Leica Biosystems) using a 63 \times /1.40 NA oil immersion objective, and images were analyzed using ImageJ. Polarization of the MTOC was assessed by measuring the ratio of the distance from the MTOC to the synapse to the distance from the synapse to the back of the cell.

Imaging of signaling proteins and actin ring formation

Chambered coverglass slides (Lab-Tek II, Nunc) were coated with 0.01% PLL (Sigma) for 20 min at room temperature, before

being washed with water and dried for 1 h at 60°C. Stimulating mAb or recombinant proteins were coated at various concentrations in PBS onto the PLL-coated slides, overnight at 4°C. mAb used were: anti-NKp30 (5 $\mu\text{g}/\text{mL}$; MAB1849; R&D), anti-CD16 (5 $\mu\text{g}/\text{mL}$; 3G8, BD Biosciences), and recombinant proteins: His-ICAM-1 (2.5 $\mu\text{g}/\text{mL}$; Peak Proteins), Fc-MICA (2.5 $\mu\text{g}/\text{mL}$; Manchester Institute of Biotechnology). Slides were washed with PBS and 100,000 NK cells were added to each well for 5 or 20 min, as required, at 37°C. Cells were fixed in 4% PFA (ThermoFisher) for 20 min at room temperature and then washed with PBS. For staining of surface proteins, cells were blocked with 1% BSA (Sigma) and 1% human serum (ThermoFisher) in PBS for 1 h at room temperature. Cells were then stained in a blocking buffer containing AF488 anti-phospho-CD3 ζ mAb (K25-407.69; BD Biosciences) and AF647 anti-phospho-Zap-70 mAb (#2701; Cell Signaling Technology) overnight at 4°C and then washed in PBS for imaging. Anti-phospho-CD3 ζ mAb was conjugated in-house with AF488 esters (Invitrogen) and desalted with Zeba spin columns (Thermo Scientific). Total internal reflection fluorescent microscopy was performed on an inverted microscope (Leica SR 3D-GSD) fitted with a HC PL APO 160X oil immersion lens (NA 1.43) and an EMCCD camera (Andor iXon Ultra 897). For imaging of synaptic actin, cells were permeabilized with 0.1% Triton X-100 (Sigma) for 10 min prior to blocking. After blocking, cells were stained with Phalloidin-AF488 (Life Technologies) for 1 h at room temperature. Cells were imaged using a Leica TCS SP8 inverted confocal microscope with a 100 \times /1.4 NA oil immersion objective (SP8, Leica Biosystems). All images were analyzed using ImageJ.

Shadow imaging

Coated slides were prepared as before with PLL and stimulating mAb or recombinant proteins. NK cells were incubated on coated slides (100,000 cells per well) for 1 h at 37°C before being gently washed with PBS. Slides were then stained with AF488 anti-ICAM-1 mAb (HCD54; BioLegend) for 1 min and washed with PBS. Cells were detached using a nonenzymatic cell-dissociation solution (Sigma-Aldrich) for 20 min at 37°C and washed with PBS. Slides were then blocked with 1% BSA (Sigma-Aldrich) and 1% human serum (ThermoFisher Scientific) in PBS for 1 h at room temperature and stained with AF647 anti-perforin mAb (dG9; BioLegend) for 1 h. Slides were finally washed with PBS and imaged on an Eclipse Ti inverted microscope (Nikon) using an Apo total internal reflection fluorescent 100 \times /1.49 NA oil objective. Images were analyzed using ImageJ.

Statistical analysis

All statistical analysis was performed using GraphPad Prism 9 (GraphPad Software). For each data set a Shapiro–Wilk test was used to test for a normal distribution. Significant differences were determined as described in figure legends using paired Student's

t-tests on biological replicates. Statistically significant differences were defined as $P < 0.05$ (*), $P < 0.01$ (**), and $P < 0.001$ (***). When $P > 0.05$, no significant differences (ns) were determined. Figures show mean \pm SD.

Acknowledgments: The authors thank everyone in the Davis laboratory for the discussion, Kevin Stacey, Judit Gali Moya, and Alicia Evans for cell isolations, and Sam Sheppard for critical appraisal of the manuscript. The authors also thank Ian Donaldson and Andy Hayes of the Bioinformatics and Genomic Technologies Core Facilities at the University of Manchester and Agrin Moeini in the Zelenay laboratory for providing support with RNA-sequencing analysis. This study was funded by Cancer Research UK via funding to the Cancer Research UK Manchester Institute (awarded to CP: C5759/A29289), a Wellcome Trust Investigator Award (to DMD; 110091/Z/15/Z), a program grant from the Medical Research Council (to DMD; MR/W031698/1), and by the Manchester Collaborative Centre for Inflammation Research (funded by a precompetitive open-innovation award from GSK, AstraZeneca, and The University of Manchester, United Kingdom).

Author Contributions: Chloe Patterson designed and performed experiments, analyzed data, and wrote the manuscript. Khodor S. Hazime helped to design experiments and performed experiments to test NK cell conjugation. Santiago Zelenay and Daniel M. Davis supervised the study, helped design experiments, and wrote the manuscript.

Conflict of Interest: The authors declare no conflict of interest.

Data availability statement: RNA sequencing data is openly available in Array Express at <https://www.ebi.ac.uk/biostudies/> reference number: E-MTAB-13106. The other datasets generated and analyzed during the current study are available from the corresponding author upon reasonable request.

Peer review: The peer review history for this article is available at <https://publons.com/publon/10.1002/eji.202350635>

References

- Caligiuri, M. A., Human natural killer cells. *Blood* 2008. **112**: 461–469.
- Anft, M., Netter, P., Urlaub, D., Prager, I., Schaffner, S. and Watzl, C., NK cell detachment from target cells is regulated by successful cytotoxicity and influences cytokine production. *Mol. Immunol.* 2020, **17**: 347–355.
- Colonna, M., Nakajima, H., Navarro, F. and López-Botet, M., A novel family of Ig-like receptors for HLA class I molecules that modulate function of lymphoid and myeloid cells. *J. Leukocyte Biol.* 1999. **66**: 375–381.
- Orange, J. S., Formation and function of the lytic NK-cell immunological synapse. *Nat. Rev. Immunol.* 2008. **8**: 713–725.
- Davis, D. M., Chiu, I., Fassett, M., Cohen, G. B., Mandelboim, O. and Strominger, J. L., The human natural killer cell immune synapse. *Proc. Natl. Acad. Sci.* 1999. **96**: 15062–15067.
- Bonavita, E., Bromley, C. P., Jonsson, G., Pelly, V. S., Sahoo, S., Walwyn-Brown, K., Mensurado, S. et al., Antagonistic inflammatory phenotypes dictate tumor fate and response to immune checkpoint blockade. *Immunity* 2020. **53**: 1215–1229.e8.
- Bottcher, J. P., Bonavita, E., Chakravarty, P., Blees, H., Cabeza-Cabrerizo, M., Sammicheli, S., Rogers, N. C. et al., NK cells stimulate recruitment of cDC1 into the tumor microenvironment promoting cancer immune control. *Cell*. 2018. **172**: 1022–10337.e14.
- Barry, K. C., Hsu, J., Broz, M. L., Cueto, F. J., Binnewies, M., Combes, A. J., Nelson, A. E. et al., A natural killer-dendritic cell axis defines checkpoint therapy-responsive tumor microenvironments. *Nat. Med.* 2018. **24**: 1178–1191.
- Souza-Fonseca-Guimaraes, F., Cursons, J. and Huntington, N. D., The emergence of natural killer cells as a major target in cancer immunotherapy. *Trends Immunol.* 2019. **40**: 142–158.
- Coca, S., Perez-Piqueras, J., Martinez, D., Colmenarejo, A., Saez, M. A., Vallejo, C., Martos, J. A. et al., The prognostic significance of intratumoral natural killer cells in patients with colorectal carcinoma. *Cancer* 1997. **79**: 2320–2328.
- Zhang, S., Liu, W., Hu, B., Wang, P., Lv, X., Chen, S. and Shao, Z., Prognostic significance of tumor-infiltrating natural killer cells in solid tumors: a systematic review and meta-analysis. *Front Immunol.* 2020. **11**: 1242.
- Martinet, L., Jean, C., Dietrich, G., Fourmié, J.-J. and Poupot, R., PGE2 inhibits natural killer and $\gamma\delta$ T cell cytotoxicity triggered by NKR and TCR through a cAMP-mediated PKA type I-dependent signaling. *Biochem. Pharmacol.* 2010. **80**: 838–845.
- Pang, L. Y., Hurst, E. A. and Argyle, D. J., Cyclooxygenase-2: a role in cancer stem cell survival and repopulation of cancer cells during therapy. *Stem cells international* 2016. **2016**: 2048731.
- Wang, D. and Dubois, R. N., Eicosanoids and cancer. *Nat. Rev. Cancer* 2010. **10**: 181–193.
- de Groot, D. J., de Vries, E. G., Groen, H. J. and de Jong, S., Non-steroidal anti-inflammatory drugs to potentiate chemotherapy effects: from lab to clinic. *Crit. Rev. Oncol. Hematol.* 2007. **61**: 52–69.
- Nakanishi, M. and Rosenberg, D. W., Multifaceted roles of PGE2 in inflammation and cancer. *Semin. Immunopathol.* 2013. **35**: 123–137.
- Park, A., Lee, Y., Kim, M. S., Kang, Y. J., Park, Y. J., Jung, H., Kim, T.-D. et al., Prostaglandin E2 secreted by thyroid cancer cells contributes to immune escape through the suppression of natural killer (NK) cell cytotoxicity and NK cell differentiation. *Front. Immunol.* 2018. **9**: 1859.
- Holt, D. M., Ma, X., Kundu, N., Collin, P. D. and Fulton, A. M., Modulation of host natural killer cell functions in breast cancer via prostaglandin E2 receptors EP2 and EP4. *J. Immunother* 2012. **35**: 179–188.
- Tóth, J. and Kubeš, M., Masking of HLA class I molecules expressed on K-562 target cells can restore their susceptibility to NK cell cytotoxicity. *Immunobiology* 1993. **188**: 134–144.
- Wang, R., Jaw, J. J., Stutzman, N. C., Zou, Z. and Sun, P. D., Natural killer cell-produced IFN- γ and TNF- α induce target cell cytotoxicity through up-regulation of ICAM-1. *J. Leukoc Biol.* 2012. **91**: 299–309.
- Lisovsky, I., Isitman, G., Bruneau, J. and Bernard, N. F., Functional analysis of NK cell subsets activated by 721.221 and K562 HLA-null cells. *J. Leukocyte Biol.* 2015. **97**: 761–767.
- BroadInstitute. Cancer Cell Line Encyclopedia. In: Institute B, editor. Online. 2020.

- 23 Chen, Z., Yang, Y., Neo, S. Y., Shi, H., Chen, Y., Wagner, A. K., Larsson, K. et al., Phosphodiesterase 4A confers resistance to PGE2-mediated suppression in CD25(+)/CD54(+) NK cells. *EMBO Rep.* 2021. 23: e51329.
- 24 Prager, I., Liesche, C., van Ooijen, H., Urlaub, D., Verron, Q., Sandström, N., Fasbender, F. et al., NK cells switch from granzyme B to death receptor-mediated cytotoxicity during serial killing. *J. Exp. Med.* 2019. 216: 2113–2127.
- 25 Terrén, I., Astarloa-Pando, G., Amarilla-Irusta, A. and Borrego, F., Chapter 3 - P815-based redirected degranulation assay to study human NK cell effector functions. In: Thomas, C., Galluzzi, L., editors. *Methods Cell Biol.* 173: Academic Press; 2023. p. 33–48.
- 26 Nicoletti, I., Migliorati, G., Pagliacci, M. C., Grignani, F. and Riccardi, C., A rapid and simple method for measuring thymocyte apoptosis by propidium iodide staining and flow cytometry. *J. Immunol. Methods* 1991. 139: 271–279.
- 27 Subramanian, A., Tamayo, P., Mootha, V. K., Mukherjee, S., Ebert, B. L., Gillette, M. A., et al., Gene set enrichment analysis: a knowledge-based approach for interpreting genome-wide expression profiles. *Proc. Natl. Acad. Sci.* 2005;102: 15545–15550.
- 28 Liberzon, A., Subramanian, A., Pinchback, R., Thorvaldsdóttir, H., Tamayo, P. and Mesirov, J. P., Molecular signatures database (MSigDB) 3.0. *Bioinformatics* 2011. 27: 1739–1740.
- 29 Pierpont, T. M., Limper, C. B. and Richards, K. L., Past, present, and future of rituximab—the world's first oncology monoclonal antibody therapy. *Front. Oncol.* 2018. 8.
- 30 Paul, S. and Lal, G., The molecular mechanism of natural killer cells function and its importance in cancer immunotherapy. *Front. Immunol.* 2017, 8: 1124.
- 31 Culley, F. J., Johnson, M., Evans, J. H., Kumar, S., Crilly, R., Casasbuenas, J., Schnyder, T. et al., Natural killer cell signal integration balances synapse symmetry and migration. *PLoS Biol.* 2009. 7: e1000159.
- 32 Rak, G. D., Mace, E. M., Banerjee, P. P., Svitkina, T. and Orange, J. S., Natural killer cell lytic granule secretion occurs through a pervasive actin network at the immune synapse. *PLoS Biol.* 2011. 9: e1001151.
- 33 Lagrue, K., Carisey, A., Oszmiana, A., Kennedy, P. R., Williamson, D. J., Cartwright, A., Barthen, C. et al., The central role of the cytoskeleton in mechanisms and functions of the NK cell immune synapse. *Immunol. Rev.* 2013. 256: 203–221.
- 34 McCann, F. E., Vanherberghen, B., Eleme, K., Carlin, L. M., Newsam, R. J., Goulding, D. and Davis, D. M., The size of the synaptic cleft and distinct distributions of filamentous actin, ezrin, CD43, and CD45 at activating and inhibitory human NK cell immune synapses. *J. Immunol.* 2003. 170: 2862–2870.
- 35 Carisey, A. F., Mace, E. M., Saeed, M. B., Davis, D. M. and Orange, J. S., Nanoscale dynamism of actin enables secretory function in cytolytic cells. *Curr Biol.* 2018. 28: 489–502.e9.
- 36 Brown, A. C. N., Oddos, S., Dobbie, I. M., Alakoskela, J.-M., Parton, R. M., Eissmann, P., Neil, M. A. A. et al., Remodelling of cortical actin where lytic granules dock at natural killer cell immune synapses revealed by super-resolution microscopy. *PLoS Biol.* 2011. 9: e1001152.
- 37 Mace, E. M., Dongre, P., Hsu, H.-T., Sinha, P., James, A. M., Mann, S. S., Forbes, L. R. et al., Cell biological steps and checkpoints in accessing NK cell cytotoxicity. *Immunology & Cell Biology* 2014. 92: 245–255.
- 38 Chen, X., Allan, D. S. J., Krzewski, K., Ge, B., Kopcow, H. and Strominger, J. L., CD28-stimulated ERK2 phosphorylation is required for polarization of the microtubule organizing center and granules in YTS NK cells. *Proc. Natl. Acad. Sci. U.S.A.* 2006. 103: 10346–10351.
- 39 Bryceson, Y. T., March, M. E., Barber, D. F., Ljunggren, H. G. and Long, E. O., Cytolytic granule polarization and degranulation controlled by different receptors in resting NK cells. *J. Exp. Med.* 2005. 202: 1001–1012.
- 40 Barber, D. F., Faure, M. and Long, E. O., LFA-1 contributes an early signal for NK cell cytotoxicity. *J. Immunol. (Baltimore, Md : 1950)* 2004. 173: 3653–3659.
- 41 Mace, E. M., Monkley, S. J., Critchley, D. R. and Takei, F., A dual role for Talin in NK cell cytotoxicity: activation of LFA-1-mediated cell adhesion and polarization of NK cells. *J. Immunol.* 2009. 182: 948–956.
- 42 Gross, C. C., Brzostowski, J. A., Liu, D. and Long, E. O., Tethering of intercellular adhesion molecule on target cells is required for LFA-1-dependent NK cell adhesion and granule polarization. *J. Immunol. (Baltimore, Md : 1950)*. 2010. 185: 2918–2926.
- 43 Ambrose, A. R., Hazime, K. S. and Davis, D. M., Analyzing single cell secretions by “shadow imaging”. In: Baldari, C. T., Dustin, M. L., editors. *The immune synapse: methods and protocols*. New York, NY: Springer US; 2023. p. 409–420.
- 44 Ambrose, A. R., Hazime, K. S., Worboys, J. D., Niembro-Vivanco, O. and Davis, D. M., Synaptic secretion from human natural killer cells is diverse and includes supramolecular attack particles. *Proc. Natl. Acad. Sci.* 2020. 117: 23717–23720.
- 45 Dechantsreiter, S., Ambrose, A. R., Worboys, J. D., Lim, J. M. E., Liu, S., Shah, R., Montero, M. A. et al., Heterogeneity in extracellular vesicle secretion by single human macrophages revealed by super-resolution microscopy. *J Extracell Vesicles* 2022. 11: e12215.
- 46 Friedman, D., Simmonds, P., Hale, A., Bere, L., Hodson, N. W., White, M. R. H. and Davis, D. Natural killer cell immune synapse formation and cytotoxicity are controlled by tension of the target interface. *J. Cell Sci.* 2021. 134: jcs258570.
- 47 Kwak, K., Sohn, H., George, R., Torgbor, C., Manzella-Lapeira, J., Brzostowski, J. and Patapoutian, A., B cell responses to membrane-presented antigens require the function of the mechanosensitive cation channel Piezo1. *Sci. Signal* 2023. 16: eabq5096.
- 48 Zelenay, S., van der Veen, A. G., Bottcher, J. P., Snelgrove, K. J., Rogers, N., Acton, S. E., Chakravarty, P. et al., Cyclooxygenase-dependent tumor growth through evasion of immunity. *Cell* 2015. 162: 1257–12570.
- 49 Eitler, J., Wotschel, N., Miller, N., Boissel, L., Klingemann, H. G., Wels, W. and Tonn, T., Inability of granule polarization by NK cells defines tumor resistance and can be overcome by CAR or ADCC mediated targeting. *J Immunother Cancer* 2021. 9: e001334.
- 50 Portillo, A. L., Hogg, R., Poznanski, S. M., Rojas, E. A., Cashell, N. J., Hammill, J. A., Chew, M. V. et al., Expanded human NK cells armed with CAR uncouple potent anti-tumor activity from off-tumor toxicity against solid tumors. *iScience* 2021. 24: 102619.
- 51 Bronger, H., Kraeft, S., Schwarz-Boeger, U., Cerny, C., Stöckel, A., Avril, S., Kiechle, M. et al., Modulation of CXCR3 ligand secretion by prostaglandin E 2 and cyclooxygenase inhibitors in human breast cancer. *Breast Cancer Res.* 2012. 14.
- 52 Bronger, H., Singer, J., Windmüller, C., Reuning, U., Zech, D., Delbridge, C., Dorn, J., et al. CXCL9 and CXCL10 predict survival and are regulated by cyclooxygenase inhibition in advanced serous ovarian cancer. *Br. J. Cancer* 2016;115: 553–563.
- 53 Müller, N., Michen, S., Tietze, S., Töpfer, K., Schulte, A., Lamszus, K., Schmitz, M. et al., Engineering NK cells modified with an EGFRVIII-specific chimeric antigen receptor to overexpress CXCR4 improves immunotherapy of CXCL12/SDF-1 α -secreting glioblastoma. *J. Immunother* 2015. 38: 197–210.

- 54 Mayol, K., Biajoux, V., Marvel, J., Balabanian, K. and Walzer, T., Sequential desensitization of CXCR4 and S1P5 controls natural killer cell trafficking. *Blood* 2011. **118**: 4863–4871.
- 55 Bernardini, G., Sciumè, G., Bosisio, D., Morrone, S., Sozzani, S. and Santoni, A., CCL3 and CXCL12 regulate trafficking of mouse bone marrow NK cell subsets. *Blood* 2008. **111**: 3626–3634.
- 56 Bonanni, V., Antonangeli, F., Santoni, A. and Bernardini, G., Targeting of CXCR3 improves anti-myeloma efficacy of adoptively transferred activated natural killer cells. *J. Immunother. Cancer* 2019. **7**: 290.
- 57 Vianello, F., Papeta, N., Chen, T., Kraft, P., White, N., Hart, W. K., Kircher, M. F. et al., Murine B16 melanomas expressing high levels of the chemokine stromal-derived factor-1/CXCL12 induce tumor-specific T cell chemorepulsion and escape from immune control. *J. Immunol.* 2006. **176**: 2902–2914.
- 58 Sanseviero, E., O'Brien, E. M., Karras, J. R., Shabaneh, T. B., Aksoy, B. A., Xu, W., Zheng, C. et al., Anti-CTLA-4 activates intratumoral NK cells and combined with IL15/IL15R α complexes enhances tumor control. *Cancer Immunol Res.* 2019. **7**: 1371–1380.
- 59 Fast, E. M., Durand, E. M., Sporrij, A., Ojeaburu, L., Maher, R., Binder, V., Gimenez, G. et al., A short pulse of prostaglandin E2 (PGE2) induces long

term chromatin changes in hematopoietic stem cells leading to increased self-renewal and engraftment. *Blood*. 2015. **126**: 246.

Abbreviations: CAR: chimeric antigen receptor · CTV: CellTrace Violet · FMI: forward migration index · MTOC: microtubule organizing center · NK: natural killer · PFA: paraformaldehyde · PGE₂: prostaglandin E₂ · TME: tumor microenvironment

Full correspondence: Prof. Daniel M. Davis, Department of Life Sciences, Imperial College London, Sir Alexander Fleming Building, South Kensington, London SW7 2AZ, United Kingdom.
e-mail: d.davis@imperial.ac.uk

Received: 29/6/2023

Revised: 4/12/2023

Accepted: 5/12/2023

Accepted article online: 7/12/2023